Strong Interlayer Magnon-Magnon Coupling in Magnetic Metal-Insulator Hybrid Nanostructures

Jilei Chen,[1,*] Chuanpu Liu,[1,*] Tao Liu,[2,*] Yang Xiao,[3,*] Ke Xia,[4] Gerrit E. W. Bauer,[5,6] Mingzhong Wu,[2] and Haiming Yu[1,†]

[1]*Fert Beijing Institute, BDBC, School of Electronic and Information Engineering, Beihang University, Xueyuan Road 37, Beijing 100191, China*

[2]*Department of Physics, Colorado State University, Fort Collins, Colorado 80523, USA*

[3]*Department of Applied Physics, Nanjing University of Aeronautics and Astronautics, Nanjing 210016, China*

[4]*Department of Physics, Beijing Normal University, Beijing 100875, China*

[5]*Institute for Materials Research, WPI-AIMR and CSNR, Tohoku University, Sendai 980-8577, Japan*

[6]*Zernike Institute for Advanced Materials, University of Groningen, Nijenborgh 4, 9747 AG Groningen, The Netherlands*

(Received 2 October 2017; revised manuscript received 7 February 2018; published 23 May 2018)

We observe strong interlayer magnon-magnon coupling in an on-chip nanomagnonic device at room temperature. Ferromagnetic nanowire arrays are integrated on a 20-nm-thick yttrium iron garnet (YIG) thin film strip. Large anticrossing gaps up to 1.58 GHz are observed between the ferromagnetic resonance of the nanowires and the in-plane standing spin waves of the YIG film. Control experiments and simulations reveal that both the interlayer exchange coupling and the dynamical dipolar coupling contribute to the observed anticrossings. The coupling strength is tunable by the magnetic configuration, allowing the coherent control of magnonic devices.

DOI: 10.1103/PhysRevLett.120.217202

Strong couplings between photons and spins, atoms, and superconducting qubits lie at the heart of realizing the quantum manipulation in quantum dots, nitrogen-vacancy centers, and mechanical oscillators [1–5]. Cavity magnon polaritons [6–12], i.e., the hybrid state of a cavity photon and a spin-wave excitation in a magnet in the cavity, have been evidence of such coupling at both ultralow and room temperatures. Strong couplings have been observed in submillimeter-sized yttrium iron garnet (YIG) spheres [10–12], which obeyed the size scaling law proposed by Dicke [13], i.e., $g \propto \sqrt{N}$ with N the number of spins. However, Dicke's law implies weak couplings when magnets become small in nanomagnonic devices [14–22], disqualifying microwaves for coherent control at the nanoscale.

Here, we report the realization of strong coupling of magnons not in photonic but magnonic cavities with standing magnon modes. This is an analog to the magnon polariton, but the cavity mode is magnonic rather than photonic, and it happens on a smaller length scale. We observe anticrossing gaps as large as 1.58 GHz at a frequency of about 7.5 GHz in heterostructures consisting of a metallic ferromagnet wire array on top of a thin-film magnetic insulator YIG. This large anticrossing gap approaches the ultrastrong coupling regime, comparable to what is observed for macroscopic cavity magnon polaritons [11]. We can control the coupling by the magnetization alignments, analogous to the tunable band gaps of magnonic crystals [23–30] that would be difficult to realize in photonic devices. The strong coupling between spatially separated nanomagnets offers new functionalities towards magnon transistors [31] or spin-wave logic [32].

A schematic of the nanomagnonic device is shown in Fig. 1(a). YIG thin films with thickness $t_1 = 20$ nm were grown on $Gd_3Ga_5O_{12}$ substrates by magnetron sputtering and patterned by ion beam etching to form a magnon waveguide of 90 μm width. Magnetic nanowire arrays were deposited on top of a YIG waveguide by electron beam evaporation with a thickness of t_2 (20-nm-thick nickel or

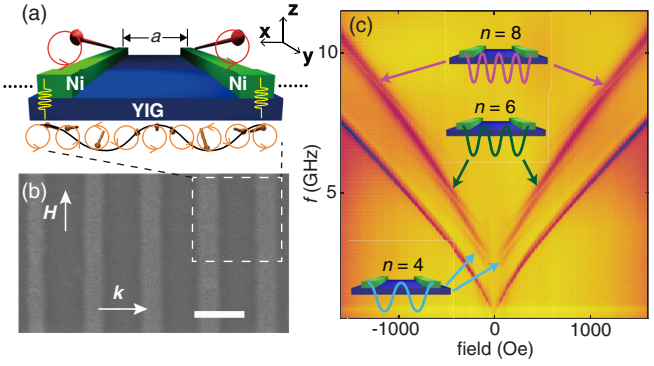

FIG. 1. (a) Sketch of a hybrid magnetic nanostructure based on a YIG thin film. The applied field H is in plane and parallel to the nanowires. (b) An SEM image (scale bar 500 nm) of the Ni-based nanowire array on YIG thin film. (c) Color-coded reflection spectra S_{11} measured on the Ni/YIG hybrid nanostructures by a coplanar waveguide. The arrows highlight anticrossing modes induced by different in-plane standing spin-wave modes with mode numbers $n = 4, 6, 8$.

30-nm-thick cobalt) [33]. a stands for the center-to-center distance of two neighboring nanowires, i.e., the period of the array. A scanning electron microscope (SEM) image of the nanomagnonic arrays with $a = 600$ nm is shown in Fig. 1(b). An external magnetic field was applied (initially) parallel to the nanowires. We excite and detect spin waves using coplanar waveguides (CPWs) integrated on top of the nanowire arrays. The scattering parameter S_{11} for reflection is measured by a vector network analyzer (VNA) connected to the CPW (Fig. S1) [33,37–40]. The nanowire arrays on top of the YIG thin film act as Bragg scattering gratings to form in-plane standing spin waves (ISSWs) with large wave numbers as illustrated in Fig. 1(a).

Figure 1(c) shows reflection spectra S_{11} measured as a function of the frequency and magnetic field where two main branches are observed. The lower-frequency branches agree with the spin-wave resonance of a bare YIG film in the Damon-Eshbach (DE) configuration [39], whereas those at higher frequencies are assigned to the ferromagnetic resonance (FMR) of the Ni wires. The Ni modes can be fitted with an in-plane demagnetization factor $N_{xx} = 0.01$ [27]. This value is smaller than the expected form factor of a wire, which has been reported also by Ding, Kostylev, and Adeyeye [41]. Dipolar interactions at the edges [42] or between neighboring wires could explain the observed reduction of the anisotropy. Here we focus on the three pronounced anticrossings (marked with arrows) observed in the Ni resonances that we attribute to the interlayer coupling between the FMR of Ni and high-order ISSWs in YIG as sketched in Fig. 1(a).

Spin waves in a periodic potential develop a band structure with gaps at the Brillouin zone boundaries with wave number π/a, where a is the unit cell length. In the limit of a strong periodic potential, the superlattice band structure becomes dispersionless, the spin waves are all localized in each unit cell, and the band index n counts the number of nodes. When the frequency of a standing spin wave in YIG approaches a resonance of the Ni wire array, a coupling results in a level repulsion or anticrossing [see Fig. 2(a)]. When the nanowires are at resonance, the strong magnetization of the relatively hard magnetic material Ni drives a spin precession in the relatively soft magnetic YIG through interlayer magnetic coupling. Since the FMR of Ni ensures in-phase precession in all nanowires, the YIG film beneath each nanowire precesses in phase as well. The associated dynamic periodic boundary conditions can be fulfilled by in-plane standing spin waves for an even number of nodes only ($n = 2$, 4, 6). In contrast, only odd-numbered perpendicular standing spin waves (PSSWs) are observed in the spin-wave resonance of intrinsic thin films [43] when there is surface pinning of the magnetization, which is not so important in the present transverse geometry. The three observed anticrossing modes in Fig. 1(c) can be fitted by dipolar-exchange spin-wave dispersion relations of YIG film [44] taking exchange

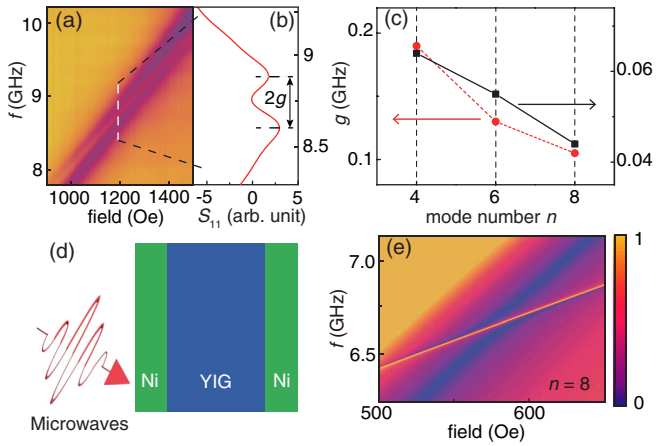

FIG. 2. (a) Color-coded reflection spectra S_{11} for high-order ISSWs with a mode number of $n = 8$. (b) The line spectrum selects the spectrum indicated by the vertical dotted line in (a) at 1200 Oe. The frequency gap in the anticrossing mode reveals the coupling strength g. (c) g as a function of the mode number $n = 4$, 6, and 8. Red dots: Experiments. Black squares: Simulations. (d) Schematic of the modeled structure. The width of YIG and Ni are 500 and 100 nm, respectively. (b) Simulation results of reflection spectra as a function of the in-plane magnetic field for the anticrossing of the Ni FMR mode and the $n = 8$ ISSW YIG mode. The color represents the reflection amplitude with the scale definition on the side.

constant $\lambda_{ex} = 3 \times 10^{-16}$ m^2 [36], the saturation magnetization $4\pi M_S = 1766$ G [20], film thickness 20 nm, and $k = n\pi/a$. As a result, these three modes are attributed to ISSWs with mode numbers $n = 4$, $n = 6$, and $n = 8$. Schematic drawings of these three high-order ISSWs are shown in the insets in Fig. 1(c). The PSSWs of the YIG films resonate at frequencies > 35 GHz and are not relevant for the present study.

In Figs. 2(a) and 2(b), an anticrossing gap of 120 MHz is observed for the $n = 8$ mode. The anticrossing covers a broad frequency range, because the Ni FMR mode and the $n = 8$ ISSW mode run nearly parallel. The coupling strength g is defined as half of the minimal peak-to-peak frequency spacing in the anticrossing. The coupling strengths g extracted for all three anticrossings are plotted in Fig. 2(c). For spin-wave resonance of films with thickness d and pinned surface magnetization [8,33], the coupling strength decreases as $g^{(n)} \propto \sqrt{d}/n$, where n is a PSSW mode number. In our case, the driving force is not the homogeneous ac field but the localized field beneath Ni nanowires. Nevertheless, with increasing n the overlap with the applied ac magnetic field is increasingly averaged out, leading to a $g \propto 1/n$ scaling as in conventional spin-wave resonance [8,33,43]. We can also extract a dissipation rate for $n = 8$ in terms of the half width at half maximum of the line broadenings as $\kappa_m^{Ni} \approx 0.63$ GHz and $\kappa_m^{YIG} \approx 0.06$ GHz. This fulfills the condition for a magnetically induced transparency (MIT) [11] for magnon transmission, since $\kappa_m^{Ni} > g > \kappa_m^{YIG}$. The magnon-magnon cooperativity

$$C = g^2/(\kappa_m^{\mathrm{Ni}} \times \kappa_m^{\mathrm{YIG}}) \quad (1)$$

is large, $C = 0.38$ in our case. Returning to the analogy with magnon polaritons, we note that the YIG magnons play the role of the cavity photons, while the Ni wire array forms the scattering object. We do not observe the scattering properties of YIG magnons directly but rather use the (auxiliary) microwave photons in order to study the coupled system. The anticrossing is caused by the periodic driving forces under the nickel FMR. Magnetization dynamics is studied in a permalloy/YIG system by the spin pumping effect not reporting anticrossing phenomena [45].

Results of model calculations of microwave absorption spectra of Ni/YIG magnetic hybrid nanostructures are shown in Fig. 2(e) for the $n = 8$ mode as an example (full simulation results are shown in Fig. S3). We consider a thin-film trilayer Ni/YIG/Ni with magnetic field driven by microwaves as shown in Fig. 2(d). This structure is a simplification of the experimental situation but captures the salient features of the observations. The PSSWs in this 1D geometry correspond to the ISSWs in the experimental structure. The reflection spectrum S_{11} shown in Fig. 2(e) is calculated by the transfer matrix method that involves solving the coupled Maxwell and Landau-Lifshitz-Gilbert equations. The SSWs are governed by magnetization boundary conditions that we chose here to be partially free (Fig. S2) [46]:

$$A\frac{\partial m_{1z}}{\partial z} - K_s m_{1z} + A_{12}\frac{M_1}{M_2} m_{2z} = 0 \quad (2)$$

with m_{nz}, M_n, A, A_{12}, and K_s being the out-of-plane component of the dynamic magnetization, saturation magnetization, exchange stiffness, interlayer exchange interaction with its neighboring layer, and interface uniaxial anisotropy field, respectively. The z axis is normal to the multilayers. In Fig. 2(e), we chose an interlayer exchange coupling between Ni and YIG of $A_{12} = 0.03$ erg/cm^2, which couples the SSWs of YIG and the FMR mode of Ni. The anticrossing gaps in Fig. 2(c) decrease with an increasing SSW mode number n, since higher-order SSWs have smaller dynamical magnetization amplitudes at the interface. The detailed analysis on the dependence of anticrossing gap on the multilayer structure, spin-wave order, and coupling mechanism will be given in a separate paper [47]. By tuning the parameters, e.g., A, A_{12}, and K_s, we find that the interlayer exchange coupling contributes to the anticrossing gap. The ferromagnetic interfacial exchange coupling in thicker YIG/ferromagnet extended bilayers has been confirmed experimentally [48–51]. For higher-order SSW modes, the interaction between SSW and FMR becomes weaker as observed [see Fig. 2(c)].

We now change the material of the nanowire array to a harder magnet (cobalt) and scale down the nanowire periodicity to 180 nm. In these samples, we measured the full spectra from −1000 to 1000 Oe [33]. The coupling strength can be controlled by varying the magnetic alignments between YIG and Co wires. Sweeping the external magnetic field gives rise to three different types of magnetization textures that characteristically modulate the reflection spectra S_{11} as shown in Fig. 3. The higher FMR frequency is caused by the larger saturation magnetization of Co compared with Ni. Figure 3(a) shows the S_{11} spectra when magnetizations of YIG and Co are parallel (denoted as the "P" state). A line plot for −450 Oe is shown in Fig. 3(b). An anticrossing appears when the Co FMR mode crosses with the $n = 4$ ISSW YIG mode. Figure 3(c) shows the extracted maxima of the resonances as well as calculated Co and YIG modes following Ref. [36]. The coupling strength g is 284 MHz. The coupling strength can be varied by the nanowire widths [33]. Compared with the Ni-based structure, the coupling strength is slightly enhanced. Nevertheless, taking into

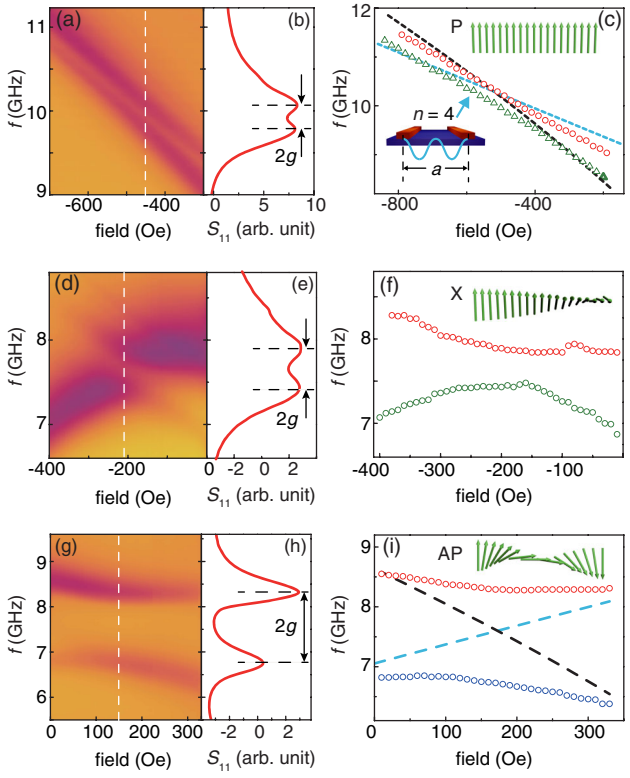

FIG. 3. (a) Color-coded reflection spectra S_{11} for the $n = 4$ ISSW mode. (b) The line spectrum is extracted at −450 Oe. (c) Data points extracted from experimental data by reading out the maxima of each resonances. The insets depict the $n = 4$ ISSW mode and the parallel state of the Co/YIG multilayer. Black dashed line: Co FMR mode. Blue dotted lines: $n = 4$ ISSW modes of YIG thin film. (a)–(c) are data for P states. (d)–(f) present data for the X state. (g)–(i) present data for the AP state of Co/YIG hybrids [33]. All data presented in this figure are data from the $n = 4$ ISSW mode.

account broadening of the Co resonance, the system is still in the MIT regime [11].

The situation changes when the magnetization becomes noncollinear. With a small external field perpendicular to the Co nanowires, their magnetizations remain along the wire axis due to a large demagnetization field [41], but the magnetization of the soft YIG layer is rotated. The size of the anticrossing gap of this magnetic configuration (denoted as the "X" state) in Figs. 3(d) and 3(e) is much larger than that of the P state. Furthermore, as shown in Figs. 3(g)–3(i), an increased magnetic field along the nanowires can even bring the YIG/Co bilayer into an antiparallel state (marked by "AP"). The full spectra of P, X, and AP states are presented in Figs. S4 and S5 [33]. The AP state exhibits a remarkably large anticrossing gap up to 1.58 GHz. One can extract from experiments $\kappa_m^{\mathrm{Co}} \approx 0.50$ GHz and $\kappa_m^{\mathrm{YIG}} \approx 0.06$ GHz away from the anticrossing. This indicates a strong coupling is formed where $g > \kappa_m^{\mathrm{Co}}$ and $g > \kappa_m^{\mathrm{YIG}}$ [11]. We can calculate a cooperativity of $C = 21$. Considering the resonance frequency $\omega_a \approx 7.5$ GHz, the coupled system yields a ratio of $g/\omega_a = 10.5\%$ that reaches the ultrastrong coupling (USC) regime (the highest USC coupling ratio achieved in Ref. [11] is 6.7%).

The USC may be attributed to the enhanced interlayer coupling strength arising from the exchange spring effect. Essential for the nanofabrication is a 1 nm-thick Ti layer between YIG and the Co/Ni nanowires that acts as an adhesive during lift-off. The Ti layer should be thin enough to ensure a ferromagnetic-type interlayer exchange coupling [52]. In the P configuration, there should be no texture, since the interlayer exchange favors the P state. As we rotate the magnetization of one of the two magnetic layers while the magnets remain collinear at the interface, we create an exchange spring near the interface that penetrates into the YIG layer over the exchange length that can be large for soft magnetic materials.

The angle-dependent measurements in Fig. 4 are additional evidence for the lateral "exchange spring." The ferromagnetic interlayer exchange coupling twists the magnetization with an increasing angle. The exchange spring is twisted by 180° in the AP configuration. The perturbation of the surface spin waves in YIG by the Co wires is then maximized, generating a large anticrossing gap. Between each step of the angular dependence measurements, the magnetic field is switched off and on in order to suppress nonuniversal effects due to the sweep history. As a consequence, the spectra in Fig. 4 are symmetric about the 180° angle. The observed collapse of the gap when reducing the magnetic field angle can be understood by the corresponding relaxation of the spring. While we are not able to observe the magnetic texture directly with our technique, this is strong evidence for an interface exchange controlled surface magnetization. A "reopen" of the gap at 0° is observed which is possibly due to the fact that at the P state 170 Oe is off the crossing point [around 450 Oe; see Figs. 3(a)–3(c)], and therefore these two modes become separated Co and YIG modes. Such a strong angular dependence may also be related to the 1D bicomponent magnonic crystal band structure [53].

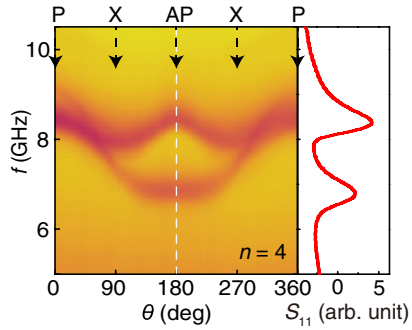

FIG. 4. Angle-dependent microwave spectra. θ is the in-plane magnetic field angle with respect to the orientation of the nanowires. At the applied field of 170 Oe, the Co wire magnetization is not modified, and the YIG magnetization is nearly parallel with the field direction. So 0° corresponds to the P and 180° to the AP state. The splitting of the lines is the anticrossing between the $n = 4$ ISSW mode and the Co FMR. A line plot at 180° is shown as an example of the color vs intensity code.

Notably, the residual mode splitting observed in the sample with a thin alumina barrier (Fig. S7) reflects a contribution from the dynamical dipolar coupling [54]. The resonance in the ferromagnetic nanowires generates oscillating magnetic charges whose stray fields interact with the YIG magnetization. The amplitude of the dynamical dipolar coupling can be estimated as $\frac{1}{2}N_{\mathrm{xx}}\gamma 4\pi M_s$ [55], which amounts to 0.83 GHz for the sample in Fig. 4. This value is not negligible compared to the interlayer exchange coupling. More precise estimations require detailed micromagnetic modeling beyond the scope of the present Letter, however.

In conclusion, we demonstrate an anticrossing between the magnon modes in ferromagnetic nanowires and the substrate formed by a magnetic insulator YIG thin film. The measured spectra prove that the FMR modes of ferromagnetic nanowires couple with high-order ISSW modes in YIG films. The coupling strength is tunable over a large range by varying the magnetization alignment of the nanowires and films. Simulations and control experiments indicate that both interlayer exchange and dynamical dipolar couplings contribute to the observed splittings. The comparison of Ni/YIG and Co/YIG hybrid nanostructures suggests that material engineering of nanomagnonic devices can enhance their functionalities.

The authors thank J. Hu, W. Zhao, Z. M. Liao, and D. P. Yu for sample fabrications and S. Tu, T. Stückler, F. Heimbach, Y. Cao, Y. Zhang, S. Granville, and B. A. Kalinikos for helpful discussions. We acknowledge the support by National Science Foundation of China under

Grant No. 11674020, youth 1000 plan, 111 talent program B16001. K. X. is supported by National Key Research and Development Program of China (Grant No. 2017YFA0303304) and the National Natural Science Foundation of China (No. 61774017, No. 11734004, and No. 21421003). T. L. and M. W. were supported by Spins and Heat in Nanoscale Electronic Systems, an Energy Frontier Research Center funded by the U.S. Department of Energy (SC0012670), and the U.S. National Science Foundation (EFMA1641989 and DMR-1407962). G. B. was supported by the Netherlands Organization for Scientific Research (NWO) and by Japan Society for the Promotion of Science Kakenhi (Japan) Grants-in-Aid for Scientific Research (Grant No. 26103006).

Note added.—Recently, reports on anticrossings in the FMR of extended bilayers between the Co Kittel mode and perpendicular standing spin waves in a micrometer-thick YIG film [56] and between the CoFeB Kittel mode and perpendicular standing spin waves in a 295-nm-thick YIG film [57] have been posted.

*These authors contributed equally to this work.
†haiming.yu@buaa.edu.cn

[1] Y. Tabuchi, S. Ishino, A. Noguchi, T. Ishikawa, R. Yamazaki, K. Usami, and Y. Nakamura, Science **349**, 405 (2015).
[2] X. Zhu, S. Shiro, A. Kemp, K. Kakuyanagi, S.-I. Karimoto, H. Nakano, W. J. Munro, Y. Tokura, M. S. Everitt, K. Nemoto, M. Kasu, N. Mizuochi, and K. Semba, Nature (London) **478**, 221 (2011).
[3] J. Majer, J. M. Chow, J. M. Gambetta, J. Koch, B. R. Johnson, J. A. Schreier, L. Frunzio, D. I. Schuster, A. A. Houck, A. Wallraff, A. Blais, M. H. Devoret, S. M. Girvin, and R. J. Schoelkopf, Nature (London) **449**, 443 (2007).
[4] A. Imamoglu, Phys. Rev. Lett. **102**, 083602 (2009).
[5] J. H. Wesenberg, A. Ardavan, G. A. D. Briggs, J. J. L. Morton, R. J. Schoelkopf, D. I. Schuster, and K. Molmer, Phys. Rev. Lett. **103**, 070502 (2009).
[6] L. Bai, M. Harder, Y. P. Chen, X. Fan, J. Q. Xiao, and C. M. Hu, Phys. Rev. Lett. **114**, 227201 (2015).
[7] H. Huebl, C. W. Zollitsch, J. Lotze, F. Hocke, M. Greifenstein, A. Marx, R. Gross, and S. T. B. Goennenwein, Phys. Rev. Lett. **111**, 127003 (2013).
[8] Y. Cao, P. Yan, H. Huebl, S. T. B. Goennenwein, and G. E. W. Bauer, Phys. Rev. B **91**, 094423 (2015).
[9] B. M. Yao, Y. S. Gui, Y. Xiao, H. Guo, X. S. Chen, W. Lu, C. L. Chien, and C. M. Hu, Phys. Rev. B **92**, 184407 (2015).
[10] J. A. Haigh, N. J. Lambert, A. C. Doherty, and A. J. Ferguson, Phys. Rev. B **91**, 104410 (2015).
[11] X. Zhang, C.-L. Zou, L. Jiang, and H. X. Tang, Phys. Rev. Lett. **113**, 156401 (2014).
[12] X. Zhang, C.-L. Zou, N. Zhu, F. Marquardt, L. Jiang, and H. X. Tang, Nat. Commun. **6**, 8914 (2015).
[13] R. H. Dicke, Phys. Rev. **93**, 99 (1954).
[14] A. V. Chumak, V. I. Vasyuchka, A. A. Serga, and B. Hillebrands, Nat. Phys. **11**, 453 (2015).
[15] D. Grundler, Nat. Nanotechnol. **11**, 407 (2016).
[16] K. Wagner, A. Kákay, K. Schultheiss, A. Henschke, T. Sebastian, and H. Schultheiss, Nat. Nanotechnol. **11**, 432 (2016).
[17] A. Khitun, M. Bao, and K. L. Wang, J. Phys. D **43**, 264005 (2010).
[18] H. Yu, O. Allivy Kelly, V. Cros, R. Bernard, P. Bortolotti, A. Anane, F. Brandl, F. Heimbach, and D. Grundler, Nat. Commun. **7**, 11255 (2016).
[19] T. Liu, H. Chang, V. Vlaminck, Y. Sun, M. Kabatek, A. Hoffmann, L. Deng, and M. Wu, J. Appl. Phys. **115**, 17A501 (2014).
[20] H. Chang, P. Li, W. Zhang, T. Liu, A. Hoffmann, L. Deng, and M. Wu, IEEE Magn. Lett. **5**, 6700104 (2014).
[21] S. Urazhdin, V. E. Demidov, H. Ulrichs, T. Kendziorczyk, T. Kuhn, J. Leuthold, G. Wilde, and S. O. Demokritov, Nat. Nanotechnol. **9**, 509 (2014).
[22] A. Haldar, D. Kumar, and A. O. Adeyeye, Nat. Nanotechnol. **11**, 437 (2016).
[23] M. Krawczyk and D. Grundler, J. Phys. Condens. Matter **26**, 123202 (2014).
[24] G. Gubbiotti, S. Tacchi, G. Carlotti, N. Singh, S. Goolaup, A. O. Adeyeye, and M. Kostylev, Appl. Phys. Lett. **90**, 092503 (2007).
[25] Z. K. Wang, V. L. Zhang, H. S. Lim, S. C. Ng, M. H. Kuok, S. Jain, and A. O. Adeyeye, ACS Nano **4**, 643 (2010).
[26] A. V. Chumak, P. Pirro, A. A. Serga, M. P. Kostylev, R. L. Stamps, H. Schultheiss, K. Vogt, S. J. Hermsdoerfer, B. Laegel, P. A. Beck, and B. Hillebrands, Appl. Phys. Lett. **95**, 262508 (2009).
[27] J. Topp, D. Heitmann, M. P. Kostylev, and D. Grundler, Phys. Rev. Lett. **104**, 207205 (2010).
[28] J. Ding, M. Kostylev, and A. O. Adeyeye, Appl. Phys. Lett. **100**, 073114 (2012).
[29] B. Obry, P. Pirro, T. Braecher, A. V. Chumak, J. Osten, F. Ciubotaru, A. A. Serga, J. Fassbender, and B. Hillebrands, Appl. Phys. Lett. **102**, 202403 (2013).
[30] G. N. Kakazei, X. M. Liu, J. Ding, and A. O. Adeyeye, Appl. Phys. Lett. **104**, 042403 (2014).
[31] A. V. Chumak, A. A. Serga, and B. Hillebrands, Nat. Commun. **5**, 4700 (2014).
[32] A. Khitun and K. L. Wang, Superlattices Microstruct. **38**, 184 (2005).
[33] See Supplemental Material at http://link.aps.org/supplemental/10.1103/PhysRevLett.120.217202 for sample fabrication details and a full device image with integrated CPWs, more information about and the results of the simulations, the measurement technique, the full spectra of the Co/YIG sample, the coupling strength dependence on Co nanowire widths, and control measurements on samples with Al_2O_3 spacers, which includes Refs. [8,34–36].
[34] W. S. Ament and G. T. Rado, Phys. Rev. **97**, 1558 (1955).
[35] S. Klingler, A. V. Chumak, T. Mewes, B. Khodadadi, C. Mewes, C. Dubs, O. Surzhenko, B. Hillebrands, and A. Conca, J. Phys. D **48**, 015001 (2015).

[36] D. D. Stancil and A. Prabhakar, *Spin Waves: Theory and Applications* (Springer, New York, 2009), Appendix C.
[37] V. Vlaminck and M. Bailleul, Science **322**, 410 (2008).
[38] S. Neusser, G. Durr, H. G. Bauer, S. Tacchi, M. Madami, G. Woltersdorf, G. Gubbiotti, C. H. Back, and D. Grundler, Phys. Rev. Lett. **105**, 067208 (2010).
[39] H. Yu, O. Allivy Kelly, V. Cros, R. Bernard, P. Bortolotti, A. Anane, F. Brandl, R. Huber, I. Stasinopoulos, and D. Grundler, Sci. Rep. **4**, 6848 (2014).
[40] S. J. Hamalainen, F. Brandl, K. J. A. Franke, D. Grundler, and S. van Dijken, Phys. Rev. Applied **8**, 014020 (2017).
[41] J. Ding, M. Kostylev, and A. O. Adeyeye, Phys. Rev. B **84**, 054425 (2011).
[42] K. Y. Guslienko, S. O. Demokritov, B. Hillebrands, and A. N. Slavin, Phys. Rev. B **66**, 132402 (2002).
[43] C. Kittel, Phys. Rev. **73**, 155 (1948).
[44] B. A. Kalinikos and A. N. Slavin, J. Phys. C **19**, 7013 (1986).
[45] P. Hyde, L. Bai, D. M. J. Kumar, B. W. Southern, C.-M. Hu, S. Y. Huang, B. F. Miao, and C. L. Chien, Phys. Rev. B **89**, 180404(R) (2014).
[46] C. Vittoria, Phys. Rev. B **37**, 2387 (1988).
[47] Y. Xiao, X. H. Yan, Y. Zhang, C. Liu, C. M. Hu, H. Guo, H. Yu, and K. Xia (to be published).
[48] Y. S. Chun and K. M. Krishnana, J. Appl. Phys. **95**, 6858 (2004).
[49] M. Pashkevich, A. Stupakiewicz, A. Kirilyuk, A. Maziewski, A. Stognij, N. Novitskii, A. Kimel, and Th. Rasing, J. Appl. Phys. **111**, 023913 (2012).
[50] N. Vukadinovic, J. Ben Youssef, V. Castel, and M. Labrune, Phys. Rev. B **79**, 184405 (2009).
[51] J. Ben Youssef, V. Castel, N. Vukadinovic, and M. Labrune, J. Appl. Phys. **108**, 063909 (2010).
[52] E. E. Shalyguina and K.-H. Shin, J. Magn. Magn. Mater. **220**, 167 (2000).
[53] C. S. Lin, H. S. Lim, Z. K. Wang, S. C. Ng, and M. H. Kuok, Appl. Phys. Lett. **98**, 022504 (2011).
[54] B. Pigeau, C. Hahn, G. de Loubens, V. V. Naletov, O. Klein, K. Mitsuzuka, D. Lacour, M. Hehn, S. Andrieu, and F. Montaigne, Phys. Rev. Lett. **109**, 247602 (2012).
[55] O. Dmytriiev, T. Meitzler, E. Bankowski, A. Slavin, and V. Tiberkevich, J. Phys. Condens. Matter **22**, 136001 (2010).
[56] S. Klingler, V. Amin, S. Geprägs, K. Ganzhorn, H. Maier-Flaig, M. Althammer, H. Huebl, R. Gross, R. D. McMichael, M. D. Stiles, S. T. B. Goennenwein, and M. Weiler, Phys. Rev. Lett. **120**, 127201 (2018).
[57] H. Qin, S. J. Hämäläinen, and S. van Dijken, Sci. Rep. **8**, 5755 (2018).